DDX41 is needed for pre- and postnatal hematopoietic stem cell differentiation in mice

Jing Ma,[1] Nadim Mahmud,[2] Maarten C. Bosland,[3] and Susan R. Ross[1,*]

[1]Department of Microbiology and Immunology, University of Illinois at Chicago College of Medicine, 835 South Wolcott Avenue, E705 MSB (MC 790), Chicago, IL 60612, USA
[2]Department of Medicine, University of Illinois at Chicago College of Medicine, Chicago, IL, USA
[3]Department of Pathology, University of Illinois at Chicago College of Medicine, Chicago, IL, USA
*Correspondence: srross@uic.edu
https://doi.org/10.1016/j.stemcr.2022.02.010

SUMMARY

DDX41 is a tumor suppressor frequently mutated in human myeloid neoplasms, but whether it affects hematopoiesis is unknown. Using a knockout mouse, we demonstrate that DDX41 is required for mouse hematopoietic stem and progenitor cell (HSPC) survival and differentiation, particularly of myeloid lineage cells. Transplantation of *Ddx41* knockout fetal liver and adult bone marrow (BM) cells was unable to rescue mice from lethal irradiation, and knockout stem cells were also defective in colony formation assays. RNA-seq analysis of Lin$^-$/cKit$^+$/Sca1$^+$ *Ddx41* knockout cells from fetal liver demonstrated that the expression of many genes associated with hematopoietic differentiation were altered. Furthermore, differential splicing of genes involved in key biological processes was observed. Our data reveal a critical role for DDX41 in HSPC differentiation and myeloid progenitor development, likely through regulating gene expression programs and splicing.

INTRODUCTION

Myelodysplastic syndrome and acute myeloid leukemia (MDS/AML) are diseases of familial and sporadic origin (Dohner et al., 2010). DEAD-box helicase 41 (*DDX41*) is commonly mutated genes in both forms (Cheah et al., 2017; Jiang et al., 2016; Lewinsohn et al., 2015; Obrochta and Godley, 2018; Polprasert et al., 2015; Sebert et al., 2019). DDX41 belongs to a family of DEAD/H box RNA helicases whose members are involved in translation, ribosome biogenesis, nuclear-cytoplasmic transport, pre-mRNA splicing, and nucleic acid sensing and pathogen recognition (Ahmad and Hur, 2015; Jankowsky, 2011; Jiang et al., 2016; Rocak and Linder, 2004; Stunnenberg et al., 2018). DDX41, which shows 99% amino acid identity in mice and humans, contains an N-terminal localization signal, a nucleic-acid-interacting DEAD box, a helicase domain, and a C-terminal Zn^{2+} finger. (Omura et al., 2016; Stavrou et al., 2018; Zhang et al., 2011). *DDX41* is a tumor suppressor; in familial MDS/AML, one mutated copy is inherited, and somatic mutations in the second allele are found in leukemic cells (Maciejewski et al., 2017).

Splicing factor (SF) mutations are common in MDS/AML, and loss of DDX41 may result in increased myeloid cell proliferation through its effects on splicing, which could cause tumor suppressor inactivation or alterations in the balance of gene isoforms in MDS/AML (Hosono, 2019; Polprasert et al., 2015). DDX41 is also a nucleic acid sensor (Stavrou et al., 2015; Zhang et al., 2011). It binds the first product of retroviral reverse transcription,

RNA/DNA hybrids, and to Stimulator of Interferon Genes (STING), initiating an anti-viral response (Stavrou et al., 2018). DDX41 also senses RNA/DNA hybrids translocated from the mitochondria during influenza A infection (Moriyama et al., 2019). That DDX41 interacts with protein and RNA/DNA hybrids in viral nucleic acid sensing and with spliceosomes suggests possible functional overlap.

We recently showed that *Ddx41* germline knockout (KO) in mice was embryonic lethal; to study its role in sensing of retroviruses, we used mice with a floxed allele (*Ddx41$^{f/f}$*) and mice with macrophage and dendritic cell-specific gene deletion (Stavrou et al., 2018). Both strains of KO mice had normal lifespans and, aside from increased susceptibility to infection with murine leukemia virus (MLV), showed no immune cell defects or cancer. Thus, lack of DDX41 in terminally differentiated macrophages did not cause transformation and suggests that the protein acts at an earlier stage in AML/MDS.

Here, we show that hematopoietic stem cell (HSC) deletion of *Ddx41* causes defects in differentiation *ex vivo* and *in vivo* and depletion of myeloid lineages. Rather than leading to increased proliferation, as has been suggested in other systems, *Ddx41* KO in mouse HSCs decreased proliferation and differentiation (Polprasert et al., 2015; Weinreb et al., 2021a, 2021b). RNA sequencing (RNA-seq) analysis of DDX41-deficient fetal liver HSCs showed profound differences in expression of genes likely to play a role in differentiation and proliferation. Thus, loss of DDX41 in HSCs does not result in a pro-oncogenic phenotype but inhibits their normal development.

RESULTS

Ddx41 knockout in HSCs causes hematopoietic defects

To create mice with DDX41-deficient HSCs, we generated *VavCre*⁺ *Ddx41*⁺/f males with one wild type (WT) and one floxed allele. Cre expression causes the loss of exons 7–9 (Figure S1A), which we showed previously results in loss of RNA, protein, and functional responses to virus infection in dendritic cells and macrophages (Stavrou et al., 2018). We used *VavCre*⁺ males because the transgene is expressed in oocytes and causes germline deletion, potentially confounding the studies (MGI, 2013) (J.M., unpublished data). The mice were mated with *Ddx41*f/f females to generate *VavCre*⁺ *Ddx41*⁻/⁻ KO, *VavCre*⁺ *Ddx41*⁺/⁻ (heterozygous; het), and WT *Ddx41*⁺/f and *Ddx41*f/f offspring. KO mice were born at the predicted mendelian frequency (Figure 1A) and were normal at birth (Figure S1B). PCR analysis of DNA isolated from B and T cells and macrophages from postnatal day 3 (PD3) KO mice showed almost complete deletion of exons 7–9 (Figure 1A). At PD3, the KO mice demonstrated failure to thrive—their growth was stunted in comparison with their WT or het littermates, and they appeared anemic (Figure S1B). No KO mice survived past PD17 (Figure 1B). By PD5, the major organs of KO mice, in particular, the spleen, were greatly reduced in size, and there were fewer erythroblasts and erythrocytes in the liver, spleen, and bone marrow (BM) (Figures S1B–S1D). Peripheral blood smears indicated anemia and complete blood cell count (CBC) analysis showed decreased leukocytes, erythrocytes, and platelets in PD3 KO mice (Figures S1D and S2A). No differences were seen between WT and het mice. Because of this lack of a difference, as well as in gene expression analysis (see below), WT and het mice were used interchangeably in this study.

We analyzed the effect of *Ddx41* loss on B, T, and myeloid cells in PD3 BM and spleen. We observed decreased cell numbers in all three populations in KO spleens, which is not surprising given the greatly reduced size of this organ (Figure S2B). The percentage of B and T cells in BM was not different between genotypes, while the myeloid cell percentage significantly decreased in the KOs (Figure 1C). Similar results were seen in PD5 BM (Figure S2C). The percentage of B cells also was not affected in PD3 and PD5 spleens, while T cells were slightly elevated at PD3 and significantly elevated at PD5 (Figures 1C and S2C). The percentage of myeloid cells in the spleens of mice of all three genotypes was decreased at PD5 compared with PD3 and was not significantly different, although 3/5 PD5 KO spleens had very low levels (Figures 1C and S2C).

During development, HSCs colonize the fetal liver, followed by translocation to neonatal BM and spleen (Ciriza et al., 2013). We next tested whether HSCs were affected by DDX41 deficiency. The HSC percentage was the same or slightly increased in PD3 KO BM and spleens compared with WT and het (Figures 1D and S2D–S2G). However, the frequency and number of Lin⁻Sca-1⁺c-Kit⁺ (LSK) cells were significantly decreased (Figures 1D and S2D). These results show that lack of DDX41 affects hematopoietic cell development as well as myeloid lineage cell differentiation.

Defects in HSC differentiation in *Ddx41* KO embryos

HSCs expand in the fetal liver from embryonic day (ED) 12.5–14.5 (Christensen et al., 2004). First, we showed that *Ddx41* RNA was expressed similarly in ED14.5 HSCs, LSKs, and LK populations (Figure 2A). We next examined the fetal liver stem cell populations in the KO mice. Like neonatal mice, HSC frequency or numbers were not affected at ED13.5 or ED14.5 (Figure 2B). However, the KO fetal liver LSK population was significantly reduced at ED14.5 but not E13.5 compared with WT or het (Figure 2B).

We further investigated lineage-committed progenitors from ED13.5 and ED14.5 KO and het fetal livers (Figure 2C). A lower percentage of granulocyte-monocyte progenitors (GMPs) and common myeloid progenitors (CMPs) in KO versus het livers was detected at both times. Neither percentages of common lymphoid progenitors (CLPs) or megakaryocyte-erythroid progenitors (MEPs) from KO fetal liver showed differences compared with het. These data show that while all LSK-derived lineages were diminished, the myeloid lineage was most affected pre- and postnatally by DDX41 loss.

DDX41-depleted HSCs fail to expand *ex vivo* and *in vivo*

We next assessed whether DDX41 deficiency affected HSC *ex vivo* differentiation and BM repopulation. In a pilot colony-forming unit (CFU) assay, we found very few colonies when 20,000 KO ED14.5 fetal liver cells were plated (not shown). To obtain sufficient KO colonies, 5-fold more KO than het cells were plated. Nonetheless, significantly fewer burst-forming unit-erythroid (BFU-E), granulocyte or macrophage progenitor (CFU-GM), and multi-potential progenitor cell granulocyte, erythrocyte, monocyte, megakaryote (CFU-GEMM) colonies were obtained with KO versus het fetal liver cells (Figure 3A). Moreover, the CFU-GM cell colonies were smaller in area, suggesting a slower proliferative rate (Figures S3A and S3B). ED14.5 LSK cells from KO fetal liver also had more cells arrested in G0 and fewer cells undergoing mitosis than those from WT or het mice (Figure 3B). KO HSCs also showed fewer dividing cells, although the difference between KO and WT/het mice was less pronounced (Figure 3B).

Next, we tested whether E14.5 fetal liver cells would repopulate the BM of lethally irradiated recipients. We transplanted 500,000 WT, het, and KO CD45.2⁺ fetal liver cells into CD45.1⁺ recipients. All recipients that received KO
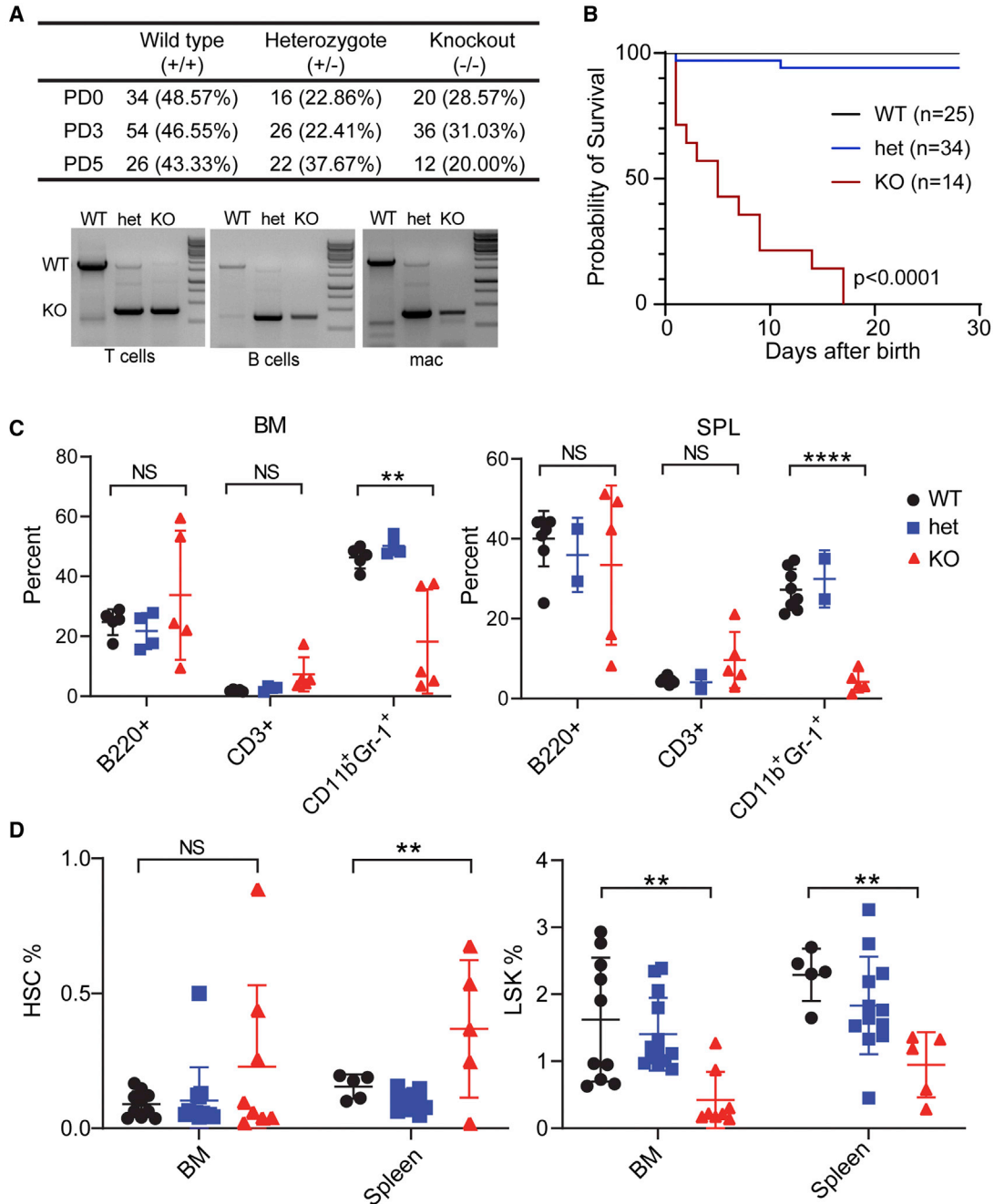
**Figure 1. *Ddx41* KO mice fail to survive postnatally**

(A) Frequency of KO mice at PD0, PD3, and PD5. Panels below show PCR analysis of DNA isolated from T and B cells and macrophages sorted from PD3 spleen of the indicated genotype pups, using primers 36 and 41 (Figure S1A). DNA is from 1 WT to one het mouse and two pooled KO mice.

(B) Postnatal survival of KO mice. p values were measured by the log rank test.

(C) Frequency of hematopoietic cells in bone marrow (BM) and spleen (SPL) at PD3.

(D) Frequency of HSPCs (LSK) decreased in KO while HSCs (LSK/CD150+/CD48−) were comparable between WT and KO PD3 mice. One-way ANOVA with *post hoc* Tukey test was used to determine significance: *, p ≤ 0.02, **, p ≤ 0.01; ***, p ≤ 0.001; ****, p ≤ 0.0001; ns, not significant. Each point represents an individual animal. For all experiments, mice were derived from a minimum of 3 litters.

See also Figure S1.
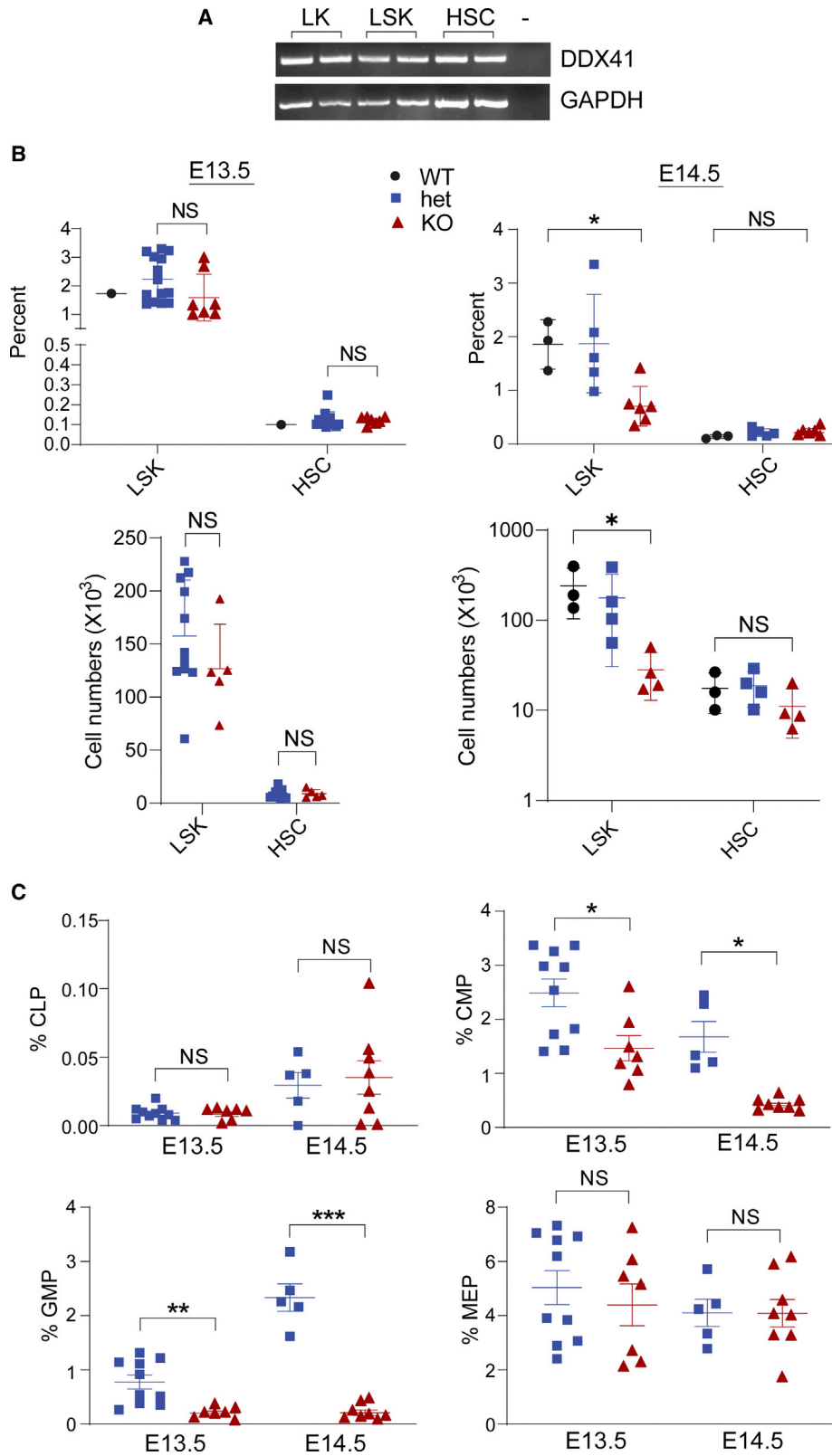
(legend on next page)

cells showed failure to thrive between 10 and 20 days after transplantation, while mice receiving WT or het BM survived, indicating that KO HSCs had limited engraftment ability (Figure 3C). We repeated the transplantation experiment by injecting 20 times more fetal liver cells (1×10^7) from KO and het embryos. Four of five KO HSC recipients failed to thrive by 17 days post-transplantation, while all recipients of WT and het HSCs were recovering, as determined by weight and CBCs (Figures S3C and S3D).

Because most KO mice were moribund, all mice were euthanized at day 17, and BM and peripheral blood were analyzed for donor cells. There were fewer donor-derived cells in the BM and blood of mice that received KO HSCs, and all three lineages (B, T, and myeloid) were decreased (Figure 3D). The failure to repopulate was not a homing defect, since at 16 h post-transplantation, equal percentages of WT and KO LSK cells were recovered from BM (Figure S3E).

We also tested whether KO HSCs isolated from adult BM repopulated lethally irradiated mice, because other studies showed that *DDX41* knockdown in adult HSCs increased their proliferation (Polprasert et al., 2015). Lineage-negative cells from 6- to 12-week-old *Ddx41 fl/fl* mice were transduced with a mouse stem cell virus (MSCV) vector expressing both Cre-recombinase and GFP, or GFP alone. The KO allele was clearly detected by PCR in cells transduced with the Cre-containing vector (Figure S3F). Fluorescence-activated cell sorting (FACS) analysis showed that 30% of LSK cells were GFP+ at 48 h post-transduction cells (Figure S3G). These cells were transplanted into lethally irradiated recipients. GFP-transduced cells were detectable in transplanted mice for up to 5 months after transplantation in all populations (total, B, T, and myeloid), while recipients that received Cre-transduced cells were gone in all populations by 1 month after transplantation (Figure 3E).

Loss of DDX41 in LSK cells alters gene expression

We next performed RNA-seq of LSK cells isolated from WT, het, and KO ED14.5 livers (three mice of each genotype); 22,320 annotated genes were analyzed. The KO mice showed significantly different gene expression levels than WT or het mice, which were similar to each other (Figures 4A and S4A). DDX41 deficiency resulted in 415 up- and 682 downregulated genes in KO versus WT/het cells (2-fold or greater) (Figure 4B and Table S1A). Gene ontology (GO) term enrichment analysis of genes more highly expressed in WT/het compared with KO LSK cells revealed signatures of inflammation, cytokine production, and adaptive immune response (top three categories), myeloid and leukocyte differentiation and activation, and neutrophil degranulation (Figure 4C). In contrast, genes involved in blood vessel development and vasculogenesis were more highly represented in KO than WT/het LSK cells (Figure 4C). Because HSCs are believed to arise from primitive endothelium, this suggests that lack of DDX41 arrests cells at an early step in the differentiation pathway.

We also found that differentially expressed transcription factors (TFs) in KO and WT/het cells were enriched in GO terms for embryonic development and cell differentiation (Figure 4D). Factors thought be important in HSC differentiation, such as GATA2 and ETV4, were slightly higher in KO cells, while CAAT/enhancer binding protein E (CEBPE), believed to play a role in granulocyte progenitor cells, and interferon regulatory factor (IRF) 4 and IRF8, which play roles in immune response, were higher in WT/het cells (Figures 4B and S4B) (Akagi et al., 2015; Nakajima et al., 2006; Tsai et al., 1994). Similarly, several cell surface receptors were differentially expressed in KO and WT/het cells, with downregulation of receptors involved in cytokine signaling, inflammatory responses, and leukocyte activation in the KO LSK population (Figures 4B, 4D and S4C).

We used RT-PCR to validate the RNA-seq data in ED14.5 LSK cells. *Vpreb2*, *Irf4*, *Irf8*, and *Clec7a*, genes involved in immune response, were more highly expressed in WT/het LSK cells, while *Edar2*, involved in ectodermal tissue development, was more highly expressed in KO cells (Figure 4E). There were also differences in *Clec7* and *Eda2r* expression in WT and KO bone-marrow-derived macrophages (BMDMs) isolated from *LysMCreDdx41 fl/fl* mice (Stavrou et al., 2018) (Figure 4F); *Vpreb2* is not expressed in macrophages. This

Figure 2. HSC defects begin prenatally in *Ddx41* KO mice

(A) LK, LSK, and HSC cells were isolated by sorting from ED14.5 fetal liver (2 mice each) and subjected to RT-qPCR with *Ddx41* primers (Table S1H). *Gapdh* RT-qPCR was used as a control.

(B) Cells isolated from prenatal liver were examined for hematopoietic stem/progenitor cells (LSK) or hematopoietic stem cells (HSCs) at day ED13.5 (KO, n = 7; het, n = 14; and WT, n = 1) and ED14.5 (KO, n = 6; het, n = 5; and WT, n = 3). The mice were derived from 3 litters for each experiment. Unpaired two-tailed t test was used for ED13.5 and one-way ANOVA with *post hoc* Tukey test was used for ED14.5 to determine significance: *, p ≤ <0.05.

(C) Cells were also examined for lineage-committed progenitor markers (CMP: Lin⁻/c-Kit⁺/Sca-1⁻/CD34⁺/CD16/32⁻; GMP: Lin⁻/c-Kit⁺/Sca-1⁻/CD34⁺/CD16/32⁺; MEP: Lin⁻/c-Kit⁺/Sca-1⁻/CD34⁻/CD16/32⁻; and CLP: Lin⁻/CD127⁺/c-Kitˡᵒʷ/Sca-1ˡᵒʷ). Unpaired two-tailed t tests were used to determine significance: *, p ≤0.05; **, p ≤0.01; ***, p ≤0.001. Each point represents an individual animal. The mice were derived from 3 litters for each experiment.
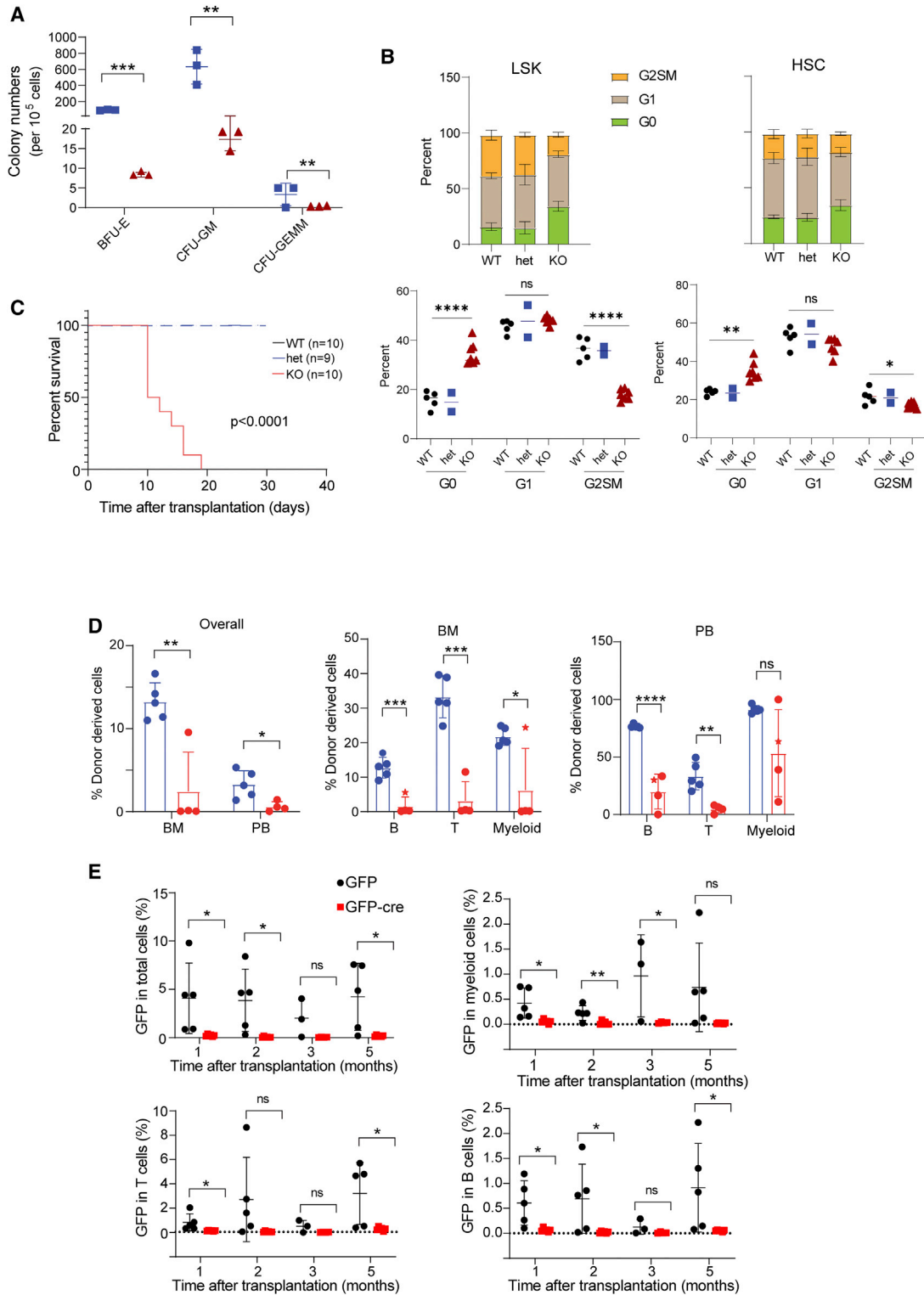
See also Figure S2.

Figure 3. HSCs from KO embryos and adult BM have compromised repopulating capacity

(A) ED14.5 fetal liver cells from KO, het, and WT mice were seeded for CFU assays. Data were collected from three independent experiments.

(B) Cell-cycle analysis of day ED14.5 fetal liver LSK and HSC cells. Each dot represents cells from an individual mouse. One way ANOVA with *post hoc* Tukey test was used for all comparisons. *, $p \leq 0.05$; **, $p \leq 0.01$; ****, $p \leq 0.0001$.

suggests that DDX41 also regulates gene expression in macrophages.

We also compared our RNA-seq data with several published datasets. First, we compared total RNA-seq data from the KO, het, and WT LSK cells with those from ED10.5 hemogenic endothelium and endothelium, ED11.5 pre-HSCs, ED14.5 fetal liver HSCs, and adult BM HSCs (Gao et al., 2020). Not surprisingly, the LSK cells from the three *Ddx41* genotypes were more like each other than any of the embryonic or adult data published dataset (Figure S4D). However, the KO LSK gene expression data were more like those from the fetal liver HSCs than were the WT or het data, suggesting that lack of DDX41 partially prevents development of cells downstream of HSCs. Indeed, the KO expression patterns had higher correlation with all the pre- and BM-HSCs analyzed by Gao et al. than did the WT or het (Figure S4D).

Several recent papers have also described expression data from adult BM *Ddx41* KO lineage-negative BM cells (Chlon et al., 2021) and from zebrafish encoding a truncated DDX41 molecule (Weinreb et al., 2021a). There was very little overlap in the over- or under-expression of genes in the FL LSK and adult lineage-negative cells, as evidenced by a comparison of GO analysis from the different datasets (Figure S4E). A comparison of GO analysis with the *ddx41* mutant zebrafish HSCs also showed no overlap (Figure S4E). In particular, while the mutant zebrafish HPSCs showed increased inflammatory signatures, we found that these pathways were decreased in KO cells (Figure S4E).

Loss of DDX41 alters splicing

DDX41 is thought to regulate splicing in human cell lines, *Caenorhabditis elegans* and zebrafish embryos (Polprasert et al., 2015; Qin et al., 2021; Tsukamoto et al., 2020; Weinreb et al., 2021a). We analyzed alternative splicing using rMATS (Tables S1B–S1F) (Shen et al., 2014). There were 367 differential splicing events between WT and KO. Skipped exons (SEs) and retained introns (RIs) were more frequently altered than alternative 5′ splice sites (A5SSs), alternative 3′ splice sites (A3SSs), or mutually exclusive exons (MXEs) in KO versus WT LSK cells (Figure 5A). GO term analysis of altered gene-splicing events (n = 350; false discovery rate [FDR] <0.05, inclusion difference >10%) revealed signatures of chromatin organization, DNA repair, mRNA processing, and cellular amide metabolism (Figure 5A). Genes with increased SEs were enriched for terms related to RNA splicing, mRNA transport, and post-translational modification (n = 175; FDR <0.05, inclusion difference >10%), while those with elevated RIs in KO cells clustered in the GO terms of ribosome biogenesis, DNA damage response, protein modification, and mRNA processing (n = 106; FDR <0.05, inclusion difference >10%) (Figures 5B–5E). Differential splicing was also found in genes encoding TFs, SFs, and receptors (Table S1G). However, there were only a few genes involved in RNA splicing/metabolism (*Srsf12*, *Rnase4*, and *Cda*) that were differentially expressed between KO and WT/het LSK cells (Table S1A).

Candidates involved in mRNA processing (*Rbm25*) and ribosome biogenesis and translation (*Abcf1*, *Imp4*, *Emg1*, and *Ptcd3*) were validated by RT-qPCR (Figures 5B–5E, S5A). Splicing of these genes was similar in WT and het. DDX41 also affected splicing in differentiated KO BMDMs from *LysMCreDdx41^{fl/fl}*, with elevated RIs in *Abcf1* and *Imp4* and increased SEs in *Ptcd3* and *Rbm25*; however, no altered splicing of *Emg1* was observed (Figure S5B).

DDX41 deficiency resulted in retention of intron 7 in *Abcf1*, intron 6 in *Imp4*, and intron 4 in *Emg1* and skipping of exon 8 in *Rbm25* and exon 14 in *Ptcd3* (Figures 5C and 5E). For *Emg1* and *Imp4*, the RI identified in KO LSK RNAs results in a premature termination codon, likely leading to transcript nonsense-mediated decay, while the *Abcf1* RI added additional in-frame coding sequences (Figure S5A). The altered splicing of *Ptcd3* and *Rbm25* resulted in in-frame proteins with exon loss (Figure 5C). Thus, altered splicing likely affected function of proteins in many pathways.

DISCUSSION

DDX41 is a nucleic sensor that binds DNA and DNA/RNA hybrids generated during virus infection (Moriyama et al., 2019; Stavrou et al., 2015, 2018; Zhang et al., 2011). Here, we show using a KO mouse model that DDX41 plays a critical role in mouse HSC survival and development and particularly disrupts the differentiation of myeloid lineage cells. DDX41 must also play a role in the maintenance and

---

(C) Transplantation of KO and het ED14.5 fetal liver cells into lethally irradiated recipients. Kaplan-Meier Curve was compared using log rank test.

(D) (Left) Percentage of donor-derived cells in BM and peripheral blood (PB) 17 days after transplantation with ED14.5 fetal liver cells. Percentage of donor-derived B cells, T cells, and myeloid cells in BM (middle) and PB (right). N ≥4 in each group of mice.

(E) Transplantation of DDX41-deficient adult bone marrow cells into lethally irradiated recipients. Percentage of donor-derived total cells, T cells, B cells, and myeloid cells in PB up to 5 months after the transplantation. N ≥3 for each group of mice. Unpaired two-tailed t tests were used to determine significance: *, p ≤0.05, **; p ≤0.01; ***, p ≤0.001; ****, p ≤0.0001. Each point represents an individual animal.
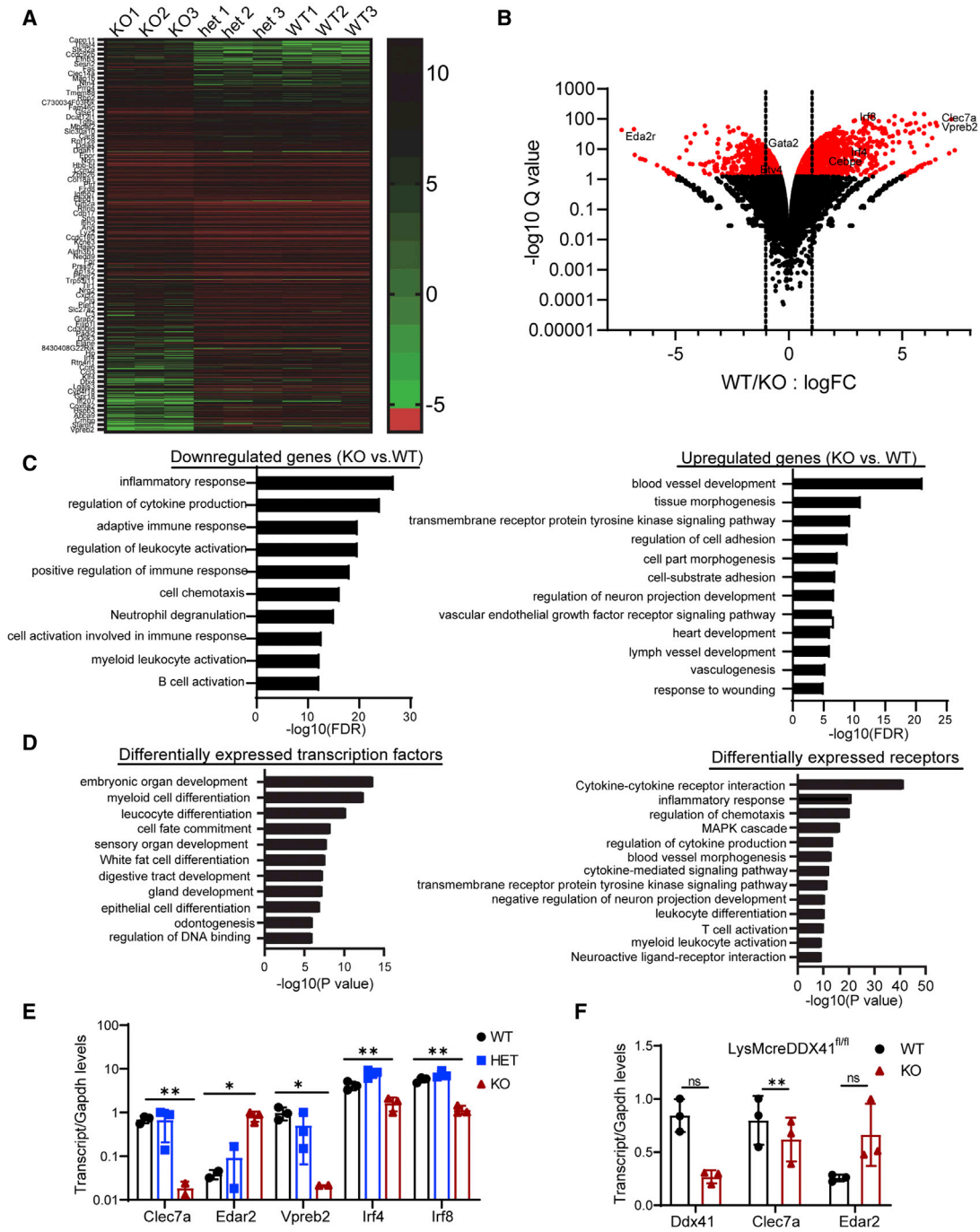
See also Figure S3.

Figure 4. DDX41 loss is linked to global alterations in gene expression

(A) Heatmap of genes differentially expressed between WT, het and KO. Log fold change (FC) ≥ 1 or ≤ -1; FDR ≤ 0.05.

(B) Volcano plot displaying differentially expressed genes between WT and KO, cutoff: logFC ≥ 1 or ≤ -1; FDR ≤ 0.01. Pseudogenes were excluded. Red points represent genes above the FDR threshold. Vertical lines separate genes by denote genes with 2-fold or greater difference. N = 3 experimental replicates per condition.

(C) Gene ontology (GO) enrichment analysis of genes higher (logFC ≥ 1) or lower represented (logFC ≤ -1) in KO versus WT. FDR ≤ 0.05.

(D) GO enrichment analysis of differentially expressed TFs and receptors. logFC (WT/KO) ≥ 1 or ≤ -1; FDR <0.05.

(legend continued on next page)

proliferation of HSCs and hematopoietic stem and progenitor cells (HSPCs), because DDX41-deficient cells were defective in both colony assays and transplantation experiments and showed a decreased capacity to proliferate. Loss of DDX41 in fetal LSK cells also led to global changes in gene expression and altered splicing, suggesting that this is how DDX41 regulates hematopoietic development.

Ddx41 KO had an effect as early as day ED14.5 when there was a loss in the percentage of fetal liver LSK cells but not HSCs. Given that HSCs constitute a subset of the LSK population, this suggests that DDX41 is required for differentiation of a progenitor population downstream of HSCs. Recent studies using single-cell RNA-seq of adult BM HSCs have indicated that this progenitor population is heterogeneous (Dong et al., 2020; Haas et al., 2018; Nestorowa et al., 2016; Wilson et al., 2015). DDX41 may be required for differentiation of a subset of the progenitor population, currently undefined by marker analysis. This could also explain why lack of DDX41 led to decreases in CMPs as early as day ED13.5. It is also interesting that both GO analysis and direct comparison of RNA-seq data with fetal liver HSCs and pre-HSCs suggests that KO LSK cells are less differentiated at ED14.5 than are WT LSK cells.

Although decreased percentages of CMP and GMP progenitors occurred at ED13.5, the myeloid lineage was not the only subset affected by lack of DDX41. While lymphoid and erythroid cell percentages were not affected in KO newborns, the absolute numbers of both subsets were decreased; the deficit in the erythroid lineage led to severe anemia, which was the likely cause of neonatal death. Given that CMPs give rise to myeloid and erythroid cells, it was unexpected that progenitor MEPs were not affected by prenatal DDX41 loss. In a parallel lineage branching model, it was proposed that heterogeneous CMPs yield only erythrocytes or myeloid cells after transplantation and that the divergence of the two lineages develops within progenitors upstream of CMP and GMP (Perie et al., 2015). DDX41 may thus be important for a subset of LSK/CMP cells that go on to contribute to the myeloid lineage. What is not known is how far back in the lineage DDX41 activity distinguishes the progenitor subset.

Inflammation is critical for HSPC proliferation and differentiation through increased expression of adhesion and hematopoietic growth factors (Granick et al., 2012; Li et al., 2020; MacNamara et al., 2011). Whole transcriptome profiling of DDX41-deficient LSK cells showed decreased expression of genes involved in inflammatory and immune

responses, which is consistent with the observation that these genes are required for HSPC differentiation. Recently, it was reported that DDX41 regulates homeostasis by suppressing the cyclic guanosine-monophosphate-adenosine monophosphate synthase (cGAS)-STING inflammatory pathway in zebrafish and human HSPCs, which is the opposite of what we observed here (Weinreb et al., 2021a, 2021b). The mutant *ddx41* gene found in the zebrafish potentially encodes a truncated protein, lacking most of the helicase domain. It is possible that this truncation causes a gain-of-function mutation leading to hyper-proliferation. Moreover, although HSC self-renewal and differentiation is highly conserved among vertebrates, zebrafish and mouse have different hematopoiesis timelines, and erythropoiesis occurs at distinct sites (de Pater and Trompouki, 2018; Kobayashi et al., 2019; Kulkeaw and Sugiyama, 2012). Thus, DDX41 may function distinctly in different species.

Whole transcriptome profiling in different species suggested that DDX41 functions in RNA splicing (Polprasert et al., 2015; Qin et al., 2021; Tsukamoto et al., 2020; Weinreb et al., 2021a). While our RNA-seq data showed that DDX41 had the greatest effects on transcript levels in LSK cells, the data also showed that DDX41 loss altered exon skipping and intron retention. In contrast to our results, in HeLa cells, A3SS, A5SS, and SEs were all regulated by DDX41, while in *C elegans* upon gene deletion, A3SS represented the predominant splicing defect (Qin et al., 2021; Tsukamoto et al., 2020). Whether these differences are species- or cell-type-specific remains to be determined. Moreover, whether defective splicing is the result of altered expression of genes, such as *Srsf12*, *Rnase4*, or *Cda* in KO cells, or the outcome of poor development can be tested by restoring WT-level expression levels through add-back or knockdown studies.

While this manuscript was under consideration, Chlon and colleagues published an analysis of *Ddx41* deletion in adult BM, in which they showed that the DDX41 was required for hematopoiesis by regulating small nucleolar RNA (snoRNA) processing and ribosome biogenesis (Chlon et al., 2021). We compared our RNA-seq analysis of fetal liver LSK cells with their analysis of adult lineage-negative *Ddx41* KO cells and found little overlap in the pathways up- or downregulated in the two sets. The lack of similarity could be due to differences in fetal versus adult stem cells, to the different populations that were examined in the two studies or because we did not select for small RNAs in our RNA-seq preparation. We did find several genes with

(E) Validation of differentially expressed genes in WT, het, and KO LSK cells by quantitative real-time PCR. Expression levels were normalized to *Gapdh*. (F) PCR validation of differentially expressed genes in WT, het, and KO BMDMs from three independent experiments. Significance was evaluated by unpaired two-tailed t test between WT and KO. *, p ≤0.05; **, p ≤0.01. N = 3 experimental replicates. See also Figure S4.
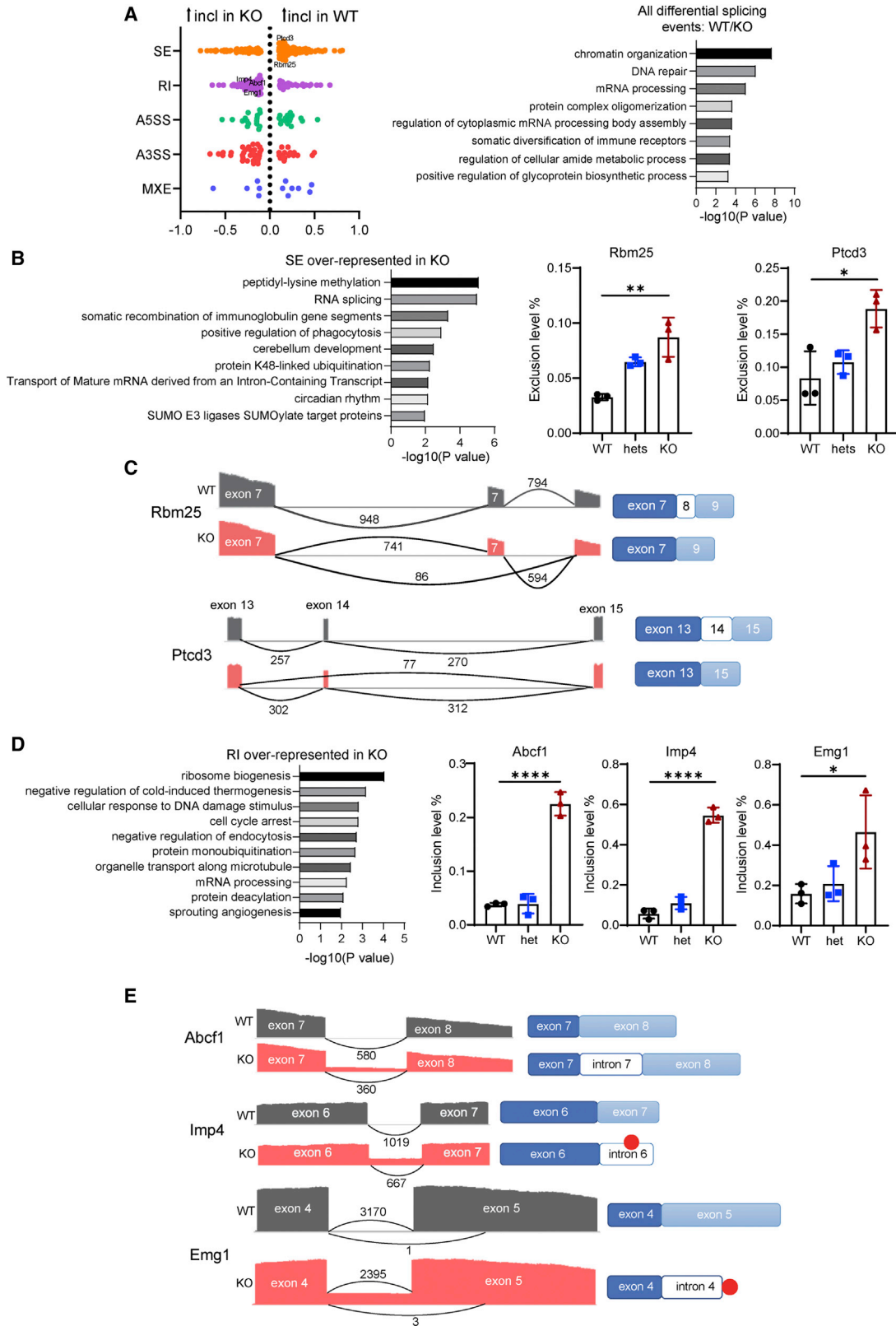
(legend on next page)

higher levels of RIs in KO cells that are involved in ribosome biogenesis and snoRNA function.

DDX41 mutations occur in familial and sporadic AML/MDS (Iacobucci et al., 2019; Lewinsohn et al., 2015; Polprasert et al., 2015). Many of these mutant alleles have the potential to encode proteins with point mutations or premature termination, which may alter their function in cells and contribute to transformation. *In silico* analysis of transcripts expressed in AML/MDS and DDX41 pull-down experiments suggested that DDX41 is involved in splicing and aberrant regulation of critical growth regulatory genes, although how it might alter splicing is not known (Polprasert et al., 2015) *DDX41* RNAi-depleted human adult CD34⁺ cells also exhibited more proliferation and greater colony formation, supporting its role in oncogenesis (Polprasert et al., 2015). Instead, we found that lack of DDX41 resulted in lower cell proliferation, loss of LSK and fully differentiated hematopoietic cells, and an inability to repopulate the BM. Cell-cycle arrest can disrupt HSC self-renewal; whether DDX41 deficiency causes HSC cell death or senescence and the mechanism by which this occurs remains to be determined. Whether the difference in proliferation is due to complete loss of DDX41 in the mouse model versus the low-level expression in the knockdown cells is not known.

It is also possible that in mouse fetal HSPCs, DDX41 plays a different role than it does in BM. Interestingly, many of the genes dysregulated in LSK cells showed similar expression and splicing patterns when DDX41 is specifically depleted from macrophages. *LysMcreDdx41^{fl/fl}* adult mice with *Ddx41* deletion in macrophages/monocytes have normal lifespans and show no phenotypic abnormalities or differences in the percentages of differentiated macrophages, and KO macrophages showed normal responses to lipopolysaccharide (LPS), polyinosinic:polycytidylic acid poly(I:C), and cyclic GMP-AMP (cGAMP) (Stavrou et al., 2018). Thus, expression of DDX41-regulated genes is apparently sufficient for differentiated macrophage function but not HSC differentiation. Moreover, loss of DDX41 in differentiated myeloid cells does not lead to their transformation.

We suggest that DDX41 regulates HSPC survival and development through its participation in transcription, perhaps by binding DNA/RNA hybrids and TFs. Simultaneously, DDX41 may act as part of splicing machinery, modulating alternative splicing leading to NMD and altering ratios of isoforms crucial to key biological processes like ribosome biogenesis, translation initiation, and mRNA processing. Finally, the affected TF, SF, and receptor translation products in turn modulate transcription and contribute to the DDX41 KO phenotype.

EXPERIMENTAL PROCEDURES

Mice and genotyping
Mice were bred at the University of Illinois at Chicago (UIC). *Ddx41^{fl/fl}* mice were constructed by TaconicArtemis and were previously described, as were *LysMCreDdx41^{fl/fl}* mice (Stavrou et al., 2018). *VavCre* (B6.Cg-Commd10Tg(Vav1-icre)A2Kio/J) mice were a gift from Kostandin Pajcini (de Boer et al., 2003). C57BL/6N and B6.SJL-Ptprca Pepcb/BoyJ (CD45.1⁺) mice were purchased from Jackson Laboratory. Both male and female mice were used for experiments, except the BM transplantation studies. Mice were housed according to the policies of the UIC Animal Care Committee (ACC); studies were performed in accordance with the recommendations in the Guide for the Care and Use of Laboratory Animals of the National Institutes of Health. The experiments were approved by UIC ACC protocol no. 21-125. Primer sequences for genotyping are in Table S1H.

Peripheral blood counts and tissue histology
Blood was collected, and CBCs were measured (Vet abc hematology analyzer [scil animal care, Gurnee, IL]). Tibiae, spleens, and livers were harvested and transferred into 10% neutral buffered formalin for 24 h fixation. Tibiae were decalcified in Immunocal overnight and then paraffin embedded. Longitudinal sections were obtained for tibiae and transverse section for spleen and liver. Five μm sections were stained with H&E and examined by light microscopy.

Figure 5. DDX41 loss results in alternative splicing
(A) Distribution of inclusion difference for major types of alternative splicing events (left). FDR <0.05; inclusion difference >10%. Types of alternative splicing events: skipped exons (SEs), alternative 5′ splice sites (A5SSs), alternative 3′ splice sites (A3SSs), mutually exclusive exons (MXEs), and retained introns (RIs). GO analysis of all differential splicing events between WT and KO (right). FDR <0.05; inclusion difference (WT/KO) ≥0.1, ≤−0.1.
(B) GO analysis of over-represented SEs in KO/WT. FDR ≤0.05; inclusion difference WT/KO ≥0.1 Splicing differences between WT, het, and KO were shown by exclusion level (the percentage of spliced-out product in both spliced-in and spliced-out products) (upper right). Significance was calculated by one-way ANOVA with *post hoc* Tukey test. *, p ≤0.05; **, p ≤0.01. N = 3 experimental replicates.
(C) Sashimi plots for *Rbm25* and *Ptcd3* in KO LSK cells compared with WT LSK cells (lower).
(D) GO analysis of over-represented RI in KO and WT cells. FDR ≤0.05; inclusion difference WT/KO ≤−0.1. Graphs representing splicing difference by inclusion level (the percentage of spliced-in product) between WT, het, and KO cells. Image Lab software (Bio-Rad) was used for gel quantification. Band intensity was normalized to *Gapdh*. Significance was evaluated by one-way ANOVA with *post hoc* Tukey test. *, p ≤0.05; ****, p ≤0.0001. N = 3 experimental replicates.
(E) Sashimi plots for *Abcf1*, *Imp4*, and *Emg1* between WT and KO. Red dots represent premature stop codons.
See also Figure S5.

Confirmation of Cre-mediated deletion

Cre-mediated deletion of exons 7–9 in *Ddx41* was confirmed by PCR (Figures 1A and S1A). Splenocytes were harvested from PD3 mice and sorted using cell surface markers for B cells (B220), T cells (CD3), and myeloid cells (CD11b Gr-1). DNA was isolated using a DNeasy Blood & Tissue Kit (QIAGEN). Specific primers flanking the two *loxP* sites were used for PCR amplification (Table S1H), and the products were analyzed by agarose gel electrophoresis.

Timed mating

Timed mating of female *Ddx41*$^{fl/fl}$ mice and male *VavCre*$^{+}$ *Ddx41*$^{fl/+}$ mice were carried out. Pregnant females were euthanized at day ED13.5 and ED14.5 and fetal liver cells were harvested for subsequent analyses.

BM and splenocyte isolation

Tibiae and femurs were dissected, and cells were collected by flushing. Livers and spleens were homogenized; red blood cells were lysed with ACK (ammonium-chloride-potassium) buffer and filtered through a 70 μm cell strainer. Single-cell suspensions were prepared in 1% fetal bovine serum (FBS) in PBS.

Flow cytometry and sorting

Cells were incubated in Fc Block (BD Biosciences) in 1% FBS-PBS and then stained with fluorescently labeled antibodies. LSK cells were identified by mouse lineage antibody cocktail (B220-FITC, CD3-FITC, CD11b-FITC, Gr-1-FITC, and Ter119-FITC), ckit-APC and Sca-1-PE. HSCs were identified by CD150-PE/Cy7, CD48-APC/Cy7, and LSK. CD16/32-APC/Cy7, CD34-PE/Cy7, LSK, and CD127-PerCp/Cy5.5 were used for analysis of lineage-committed progenitors (CMPs, GMPs, MEPs, and CLPs) (Mayle et al., 2013). CD11b-FITC and Gr-1-PE were used to stain myeloid cells. Antibody information is in Table S1I. DAPI (4′,6-diamidino-2-phenyl-indole) was added to exclude dead cells. Flow cytometry experiments were performed on a LSRFortessa (BD Biosciences) with a high-throughput sampler (HTS) and analyzed using FlowJo software. A MoFlo Astrios Cell Sorter (Beckman Coulter) was used for cell sorting; 15,000 to 20,000 LSK cells were sorted, and the purity of the populations was >98%.

Ddx41 expression

ED14.5 WT LK, LSK, and HSC cells were sorted from fetal liver. RNA was isolated using Arcturus PicoPure RNA Isolation Kit (Thermo Fisher Scientific) or RNeasy Micro Kit (QIAGEN) and then reverse-transcribed into cDNA by Super-ScriptIIIFirst-Strand Synthesis System (Invitrogen). RT-PCR was performed with primers spanning exons 6 and 7 in *Ddx41* (Table S1H), using GoTaq Master Mix systems (Promega). *Ddx41* and *Gapdh* expression were detected by agarose gel electrophoresis.

Cell-cycle analysis

Fetal liver cells from ED14.5 were first stained with cell surface marker antibodies and then fixed and permeabilized using a fixation and permeabilization solution (BD Biosciences). The cells were stained with Alexa Fluor 700-Ki-67 antibody and 7-aminoactinomycin D (AAD), followed by flow cytometry analysis.

BM rescue

Female recipient B6.SJL-Ptprca Pepcb/BoyJ mice were lethally irradiated (8.5 Gy; JL Shepherd model 143-68 cesium 137 irradiator) 1 day before transplantation. ED14.5 fetal liver cells were harvested and single-cell suspensions prepared. Cells from 2–3 mice were pooled for each genotype and were injected retro-orbitally into each recipient. Survival was monitored for up to 30 days.

MSCV transduction

Retroviral vectors were produced in HEK293T, using a three-plasmid system (MSCV-Cre-GFP [Addgene plasmid no. 24064], MLV Gag-Pol/pHit111, and MLV Env/pHIT60) (Soneoka et al., 1995). Lineage depletion of fetal liver cells was completed following the manufacturer's protocol (Miltenyi, no. 130-090-858). After culturing in stem cell media (serum-free expansion medium [SFEM] media with murine thrombopoietin [mTPO], interleukin [IL]-3, IL-6, and stem cell factor [SCF]), the cells were transduced with the MSCV-Cre-containing retrovirus. Reagent information is found in Table S1I.

Homing assays

ED14.5 liver cells were harvested from WT, het, or KO mice (CD45.2^{+}). After lineage depletion, 5×10^{5} lineage-negative cells were injected retro-orbitally into lethally irradiated B6.SJL-Ptprca Pepcb/BoyJ mice. The cells were analyzed by flow cytometry for the number of injected LSK cells. At 16 h after transplantation, recipient BM cells were analyzed by flow cytometry. The absolute number of donor-derived cells in BM was determined and the percentage of homed cells/injected cells was calculated.

Colony-forming unit assays

The protocol "Mouse Colony-Forming Unit (CFU) Assays Using MethoCultTM" (STEMCELL Technologies, Canada) was used. Fetal liver cells were harvested from ED14.5 embryos. Red blood cells were lysed, and single-cell suspensions were prepared in Iscove's Modified Dulbecco's Medium (IMDM) with 2% FBS; 20,000 to 100,000 cells were seeded in 35 mm culture dishes in duplicate culture experiments. BFU-E, CFU-GM, and CFU-GEMM colonies were identified by their morphology 12–14 days after seeding. Colonies were captured with a Keyence BZ-X710 microscope. Colony number and size were measured by BZX Analyzer software.

RNA library construction and sequencing

RNA was isolated from 1.5×10^{4} ED14.5 fetal liver LSK cells from WT, het, and KO mice (3 each) by RNeasy Micro Kit with DNase I (QIAGEN). Quality control was done by Qubit RNA assay. Library construction and sequencing were performed by Novogene (Tianjin Sequencing Center & Clinical Lab, China). cDNA synthesis was completed by SMART-Seq v.4 ultra low input RNA kit for sequencing (Clontech). Samples were sequenced on Illumina machines; paired end, 150 bp (PE150) sequencing was performed.

RNA sequencing analysis

For gene quantification, raw reads were aligned to Reference Genome mm10 in a splice-aware manner using the STAR aligner

(Dobin et al., 2013). ENSEMBL gene annotations were quantified using featureCounts (Liao et al., 2014). Differential expression statistics (fold change and p value) were computed using edgeR on raw expression counts obtained from quantification. Multi-group analyses were performed to quantify any differences between genotypes using the generalized linear models (GLMs) as well as pairwise tests between sample conditions using exactTest in edgeR (McCarthy et al., 2012; Robinson et al., 2010). Replicate multivariate analysis of transcript splicing (rMATS) was run with the default settings for the detection of differential alternative splicing events (Shen et al., 2014). To compare our RNA-seq data with those of Gao and colleagues (Gao et al., 2020), normalized gene expression data were obtained from Gene Expression Omnibus (GSE135600) and merged with our RNA-seq data based on the Ensembl ID. Spearman correlation coefficients were computed between each pair of samples, and hierarchical clustering run to compare the relative similarities between each sample. Correlation values were plotted in a heatmap (Figure S4D).

Gene ontology analysis

Metascape gene annotation and analysis resource was used to perform GO analysis (Zhou et al., 2019). P values or q values were used as representation metrics for ranking enriched terms, as indicated in the figures.

Quantitative real-time PCR and splicing validation

Total cellular RNA was isolated with RNeasy Micro Kits with DNase I (QIAGEN). cDNA was synthesized using SuperScript III First-Strand Synthesis System (Invitrogen). RNA levels in LSK cells and BMDMs were determined by real-time qPCR using SYBR Green Master Mix (Thermo Fisher Scientific) (10 min at 95°C, 40 cycles of 15 s at 95°C, and 1 min at 60°C). Mouse *Gapdh* was used as internal reference and the ΔΔCt method was used to compare expression between samples. For splicing validation, PCR was carried out with GoTaq Green Master Mix, according to the manufacturer's protocol (Promega), and products were analyzed on 4% NuSieve 3:1 agarose gels. Primer sequences designed by the National Center for Biotechnology Information (NCBI) primer-blast tool are shown in Table S1H.

Statistical analysis

Statistical analyses were performed by GraphPad Prism. Error bars represent mean ± SD. Tests used to determine significance are indicated in the figure legends. Survival curves were constructed by Kaplan-Meier analysis, and log rank test was used for comparison.

Data and code availability

No data were excluded from the analysis. Raw data are available at Mendeley Data, v.1, https://data.mendeley.com/datasets/xbr2w4mydr/1. All RNA-seq data are deposited in GEO under the accession code database GSE178979.

SUPPLEMENTAL INFORMATION

Supplemental information can be found online at https://doi.org/10.1016/j.stemcr.2022.02.010.

REFERENCES

Ahmad, S., and Hur, S. (2015). Helicases in antiviral immunity: dual properties as sensors and effectors. Trends Biochem. Sci. *40*, 576–585. https://doi.org/10.1016/j.tibs.2015.08.001.

Akagi, T., Kuure, S., Uranishi, K., Koide, H., Costantini, F., and Yokota, T. (2015). ETS-related transcription factors ETV4 and ETV5 are involved in proliferation and induction of differentiation-associated genes in embryonic stem (ES) cells. J. Biol. Chem. *290*, 22460–22473. https://doi.org/10.1074/jbc.M115.675595.

Cheah, J.J.C., Hahn, C.N., Hiwase, D.K., Scott, H.S., and Brown, A.L. (2017). Myeloid neoplasms with germline DDX41 mutation. Int. J. Hematol. *106*, 163–174. https://doi.org/10.1007/s12185-017-2260-y.

Chlon, T.M., Stepanchick, E., Hershberger, C.E., Daniels, N.J., Hueneman, K.M., Kuenzi Davis, A., Choi, K., Zheng, Y., Gurnari, C., Haferlach, T., et al. (2021). Germline DDX41 mutations cause ineffective hematopoiesis and myelodysplasia. Cell Stem Cell *28*. https://doi.org/10.1016/j.stem.2021.08.004.

Christensen, J.L., Wright, D.E., Wagers, A.J., and Weissman, I.L. (2004). Circulation and chemotaxis of fetal hematopoietic stem cells. PLoS Biol. *2*, E75. https://doi.org/10.1371/journal.pbio.0020075.

Ciriza, J., Thompson, H., Petrosian, R., Manilay, J.O., and Garcia-Ojeda, M.E. (2013). The migration of hematopoietic progenitors from the fetal liver to the fetal bone marrow: lessons learned and possible clinical applications. Exp. Hematol. *41*, 411–423. https://doi.org/10.1016/j.exphem.2013.01.009.

de Boer, J., Williams, A., Skavdis, G., Harker, N., Coles, M., Tolaini, M., Norton, T., Williams, K., Roderick, K., Potocnik, A.J., and Kioussis, D. (2003). Transgenic mice with hematopoietic and lymphoid specific expression of Cre. Eur. J. Immunol. *33*, 314–325. https://doi.org/10.1002/immu.200310005.

de Pater, E., and Trompouki, E. (2018). Bloody zebrafish: novel methods in normal and malignant hematopoiesis. Front. Cell Dev. Biol. *6*, 124. https://doi.org/10.3389/fcell.2018.00124.

Dobin, A., Davis, C.A., Schlesinger, F., Drenkow, J., Zaleski, C., Jha, S., Batut, P., Chaisson, M., and Gingeras, T.R. (2013). STAR: ultrafast universal RNA-seq aligner. Bioinformatics *29*, 15–21. https://doi.org/10.1093/bioinformatics/bts635.

Dohner, H., Estey, E.H., Amadori, S., Appelbaum, F.R., Buchner, T., Burnett, A.K., Dombret, H., Fenaux, P., Grimwade, D., Larson, R.A., et al. (2010). Diagnosis and management of acute myeloid leukemia in adults: recommendations from an international expert panel, on behalf of the European LeukemiaNet. Blood *115*, 453–474. https://doi.org/10.1182/blood-2009-07-235358.

Dong, F., Hao, S., Zhang, S., Zhu, C., Cheng, H., Yang, Z., Hamey, F.K., Wang, X., Gao, A., Wang, F., et al. (2020). Differentiation of transplanted haematopoietic stem cells tracked by single-cell transcriptomic analysis. Nat. Cell Biol. *22*, 630–639. https://doi.org/10.1038/s41556-020-0512-1.

Gao, P., Chen, C., Howell, E.D., Li, Y., Tober, J., Uzun, Y., He, B., Gao, L., Zhu, Q., Siekmann, A.F., et al. (2020). Transcriptional regulatory network controlling the ontogeny of hematopoietic stem cells. Genes Dev. *34*, 950–964. https://doi.org/10.1101/gad.338202.120.

Granick, J.L., Simon, S.I., and Borjesson, D.L. (2012). Hematopoietic stem and progenitor cells as effectors in innate immunity. Bone Marrow Res. *2012*, 165107. https://doi.org/10.1155/2012/165107.

Haas, S., Trumpp, A., and Milsom, M.D. (2018). Causes and consequences of hematopoietic stem cell heterogeneity. Cell Stem Cell *22*, 627–638. https://doi.org/10.1016/j.stem.2018.04.003.

Hosono, N. (2019). Genetic abnormalities and pathophysiology of MDS. Int. J. Clin. Oncol. *24*. https://doi.org/10.1007/s10147-019-01462-6.

Iacobucci, I., Wen, J., Meggendorfer, M., Choi, J.K., Shi, L., Pounds, S.B., Carmichael, C.L., Masih, K.E., Morris, S.M., Lindsley, R.C., et al. (2019). Genomic subtyping and therapeutic targeting of acute erythroleukemia. Nat. Genet. *51*, 694–704. https://doi.org/10.1038/s41588-019-0375-1.

Jankowsky, E. (2011). RNA helicases at work: binding and rearranging. Trends Biochem. Sci. *36*, 19–29. https://doi.org/10.1016/j.tibs.2010.07.008.

Jiang, Y., Zhu, Y., Liu, Z.J., and Ouyang, S. (2016). The emerging roles of the DDX41 protein in immunity and diseases. Protein Cell *8*. https://doi.org/10.1007/s13238-016-0303-4.

Kobayashi, I., Kondo, M., Yamamori, S., Kobayashi-Sun, J., Taniguchi, M., Kanemaru, K., Katakura, F., and Traver, D. (2019). Enrichment of hematopoietic stem/progenitor cells in the zebrafish kidney. Sci. Rep. *9*, 14205. https://doi.org/10.1038/s41598-019-50672-5.

Kulkeaw, K., and Sugiyama, D. (2012). Zebrafish erythropoiesis and the utility of fish as models of anemia. Stem cell Res. Ther. *3*, 55. https://doi.org/10.1186/scrt146.

Lewinsohn, M., Brown, A.L., Weinel, L.M., Phung, C., Rafidi, G., Lee, M.K., Schreiber, A.W., Feng, J., Babic, M., Chong, C.E., et al. (2015). Novel germline DDX41 mutations define families with a lower age of MDS/AML onset, and lymphoid malignancies. Blood *127*. https://doi.org/10.1182/blood-2015-10-676098.

Li, Y., Kong, W., Yang, W., Patel, R.M., Casey, E.B., Okeyo-Owuor, T., White, J.M., Porter, S.N., Morris, S.A., and Magee, J.A. (2020). Single-cell analysis of neonatal HSC ontogeny reveals gradual and uncoordinated transcriptional reprogramming that begins before birth. Cell Stem Cell *27*, 732–747 e737. https://doi.org/10.1016/j.stem.2020.08.001.

Liao, Y., Smyth, G.K., and Shi, W. (2014). featureCounts: an efficient general purpose program for assigning sequence reads to genomic features. Bioinformatics *30*, 923–930. https://doi.org/10.1093/bioinformatics/btt656.

Maciejewski, J.P., Padgett, R.A., Brown, A.L., and Muller-Tidow, C. (2017). DDX41-related myeloid neoplasia. Semin. Hematol. *54*, 94–97. https://doi.org/10.1053/j.seminhematol.2017.04.007.

MacNamara, K.C., Oduro, K., Martin, O., Jones, D.D., McLaughlin, M., Choi, K., Borjesson, D.L., and Winslow, G.M. (2011). Infection-induced myelopoiesis during intracellular bacterial infection is critically dependent upon IFN-gamma signaling. J. Immunol. *186*, 1032–1043. https://doi.org/10.4049/jimmunol.1001893.

Mayle, A., Luo, M., Jeong, M., and Goodell, M.A. (2013). Flow cytometry analysis of murine hematopoietic stem cells. Cytometry. A *83*, 27–37. https://doi.org/10.1002/cyto.a.22093.

McCarthy, D.J., Chen, Y., and Smyth, G.K. (2012). Differential expression analysis of multifactor RNA-Seq experiments with respect to biological variation. Nucleic Acids Res. *40*, 4288–4297. https://doi.org/10.1093/nar/gks042.

MGI (2013). Expression/Specificity Patterns of Cre Alleles (Genetic Resource Science at the Jackson Laboratory) (MGI), J:193672.

Moriyama, M., Koshiba, T., and Ichinohe, T. (2019). Influenza A virus M2 protein triggers mitochondrial DNA-mediated antiviral immune responses. Nat. Commun. *10*, 4624. https://doi.org/10.1038/s41467-019-12632-5.

Nakajima, H., Watanabe, N., Shibata, F., Kitamura, T., Ikeda, Y., and Handa, M. (2006). N-terminal region of CCAAT/enhancer-binding protein epsilon is critical for cell cycle arrest, apoptosis, and functional maturation during myeloid differentiation. J. Biol. Chem. *281*, 14494–14502. https://doi.org/10.1074/jbc.M600575200.

Nestorowa, S., Hamey, F.K., Pijuan Sala, B., Diamanti, E., Shepherd, M., Laurenti, E., Wilson, N.K., Kent, D.G., and Gottgens, B. (2016). A single-cell resolution map of mouse hematopoietic stem and progenitor cell differentiation. Blood *128*, e20–e31. https://doi.org/10.1182/blood-2016-05-716480.

Obrochta, E., and Godley, L.A. (2018). Identifying patients with genetic predisposition to acute myeloid leukemia. Best Pract. Res. Clin. Haematol. *31*, 373–378. https://doi.org/10.1016/j.beha.2018.09.014.

Omura, H., Oikawa, D., Nakane, T., Kato, M., Ishii, R., Ishitani, R., Tokunaga, F., and Nureki, O. (2016). Structural and Functional

Analysis of DDX41: a bispecific immune receptor for DNA and cyclic dinucleotide. Sci. Rep. *6*, 34756. https://doi.org/10.1038/srep34756.

Perie, L., Duffy, K.R., Kok, L., de Boer, R.J., and Schumacher, T.N. (2015). The branching point in erythro-myeloid differentiation. Cell *163*, 1655–1662. https://doi.org/10.1016/j.cell.2015.11.059.

Polprasert, C., Schulze, I., Sekeres, M.A., Makishima, H., Przychodzen, B., Hosono, N., Singh, J., Padgett, R.A., Gu, X., Phillips, J.G., et al. (2015). Inherited and somatic defects in DDX41 in myeloid neoplasms. Cancer Cell *27*, 658–670. https://doi.org/10.1016/j.ccell.2015.03.017.

Qin, K., Jian, D., Xue, Y., Cheng, Y., Zhang, P., Wei, Y., Zhang, J., Xiong, H., Zhang, Y., and Yuan, X. (2021). DDX41 regulates the expression and alternative splicing of genes involved in tumorigenesis and immune response. Oncol. Rep. *45*, 1213–1225. https://doi.org/10.3892/or.2021.7951.

Robinson, M.D., McCarthy, D.J., and Smyth, G.K. (2010). edgeR: a Bioconductor package for differential expression analysis of digital gene expression data. Bioinformatics *26*, 139–140. https://doi.org/10.1093/bioinformatics/btp616.

Rocak, S., and Linder, P. (2004). DEAD-box proteins: the driving forces behind RNA metabolism. Nat. Rev. Mol. Cell Biol. *5*, 232–241. https://doi.org/10.1038/nrm1335.

Sebert, M., Passet, M., Raimbault, A., Rahme, R., Raffoux, E., Sicre de Fontbrune, F., Cerrano, M., Quentin, S., Vasquez, N., Da Costa, M., et al. (2019). Germline DDX41 mutations define a significant entity within adult MDS/AML patients. Blood *134*. https://doi.org/10.1182/blood.2019000909.

Shen, S., Park, J.W., Lu, Z.X., Lin, L., Henry, M.D., Wu, Y.N., Zhou, Q., and Xing, Y. (2014). rMATS: robust and flexible detection of differential alternative splicing from replicate RNA-Seq data. Proc. Natl. Acad. Sci. U S A *111*, E5593–E5601. https://doi.org/10.1073/pnas.1419161111.

Soneoka, Y., Cannon, P.M., Ramsdale, E.E., Griffiths, J.C., Romano, G., Kingsman, S.M., and Kingsman, A.J. (1995). A transient three-plasmid expression system for the production of high titer retroviral vectors. Nucl. Acids Res. *23*, 628–633.

Stavrou, S., Aguilera, A.N., Blouch, K., and Ross, S.R. (2018). DDX41 recognizes RNA/DNA retroviral reverse transcripts and is critical for in vivo control of murine leukemia virus infection. MBio *9*. https://doi.org/10.1128/mBio.00923-18.

Stavrou, S., Blouch, K., Kotla, S., Bass, A., and Ross, S.R. (2015). Nucleic acid recognition orchestrates the anti-viral response to retroviruses. Cell Host Microbe *17*, 478–488. https://doi.org/10.1016/j.chom.2015.02.021.

Stunnenberg, M., Geijtenbeek, T.B.H., and Gringhuis, S.I. (2018). DDX3 in HIV-1 infection and sensing: a paradox. Cytokine Growth Factor Rev. *40*, 32–39. https://doi.org/10.1016/j.cytogfr.2018.03.001.

Tsai, F.Y., Keller, G., Kuo, F.C., Weiss, M., Chen, J., Rosenblatt, M., Alt, F.W., and Orkin, S.H. (1994). An early haematopoietic defect in mice lacking the transcription factor GATA-2. Nature *371*, 221–226. https://doi.org/10.1038/371221a0.

Tsukamoto, T., Gearhart, M.D., Kim, S., Mekonnen, G., Spike, C.A., and Greenstein, D. (2020). Insights into the involvement of spliceosomal mutations in myelodysplastic disorders from analysis of SACY-1/DDX41 in Caenorhabditis elegans. Genetics *214*, 869–893. https://doi.org/10.1534/genetics.119.302973.

Weinreb, J.T., Ghazale, N., Pradhan, K., Gupta, V., Potts, K.S., Tricomi, B., Daniels, N.J., Padgett, R.A., De Oliveira, S., Verma, A., and Bowman, T.V. (2021a). Excessive R-loops trigger an inflammatory cascade leading to increased HSPC production. Dev. Cell *56*, 627–640 e625. https://doi.org/10.1016/j.devcel.2021.02.006.

Weinreb, J.T., Gupta, V., Sharvit, E., Weil, R., and Bowman, T.V. (2021b). Ddx41 inhibition of DNA damage signaling permits erythroid progenitor expansion in zebrafish. Haematologica https://doi.org/10.3324/haematol.2020.257246.

Wilson, N.K., Kent, D.G., Buettner, F., Shehata, M., Macaulay, I.C., Calero-Nieto, F.J., Sanchez Castillo, M., Oedekoven, C.A., Diamanti, E., Schulte, R., et al. (2015). Combined single-cell functional and gene expression analysis resolves heterogeneity within stem cell populations. Cell Stem Cell *16*, 712–724. https://doi.org/10.1016/j.stem.2015.04.004.

Zhang, Z., Yuan, B., Bao, M., Lu, N., Kim, T., and Liu, Y.-J. (2011). The helicase DDX41 senses intracellular DNA mediated by the adaptor STING in dendritic cells. Nat. Immunol. *12*, 959–965. https://doi.org/10.1038/ni.2091.

Zhou, Y., Zhou, B., Pache, L., Chang, M., Khodabakhshi, A.H., Tanaseichuk, O., Benner, C., and Chanda, S.K. (2019). Metascape provides a biologist-oriented resource for the analysis of systems-level datasets. Nat. Commun. *10*, 1523. https://doi.org/10.1038/s41467-019-09234-6.